# In situ X-ray Absorption Spectroscopy in Homogeneous Conditions Reveals Interactions Between CO 2 and a Doubly and Triply Reduced Iron(III) Porphyrin, then Leading to Catalysis

Daniela Mendoza, Si-thanh Dong, Nikolaos Kostopoulos, Victor Pinty, Orestes Rivada-Wheelaghan, Elodie Anxolabéhère-Mallart, Marc Robert, Benedikt Lassalle-Kaiser

# *In situ* X-ray absorption spectroscopy in homogeneous conditions reveals interactions between $CO_2$ and a doubly and triply reduced iron(III) porphyrin, then leading to catalysis

Daniela Mendoza,[a,b] Si-Thanh Dong,[a] Nikolaos Kostopoulos,[b] Victor Pinty,[a] Orestes Rivada-Wheelaghan,[b] Elodie Anxolabéhère-Mallart*[b] Marc Robert*[b,c] and Benedikt Lassalle-Kaiser*[a]

Dedicated to the late Doris Lexa

[a] Dr. D. Mendoza, Mr. S.-T. Dong, Mr. V. Pinty and Dr. B. Lassalle-Kaiser
Science Division
Synchrotron SOLEIL
L'Orme des Merisiers, Départementale 128
91190, Saint-Aubin, France
E-mail: benedikt.lassalle@synchrotron-soleil.fr
[b] Dr. D. Mendoza, Dr. N. Kostopoulos, Dr. O. Rivada-Wheelaghan, Dr. E. Anxolabéhère-Mallart, Pr. Dr. M. Robert
Université Paris Cité, CNRS
Laboratoire d'Electrochimie Moléculaire, F-75013 Paris, France
Email : elodie.anxolabehere@u-paris.fr, robert@u-paris.fr
[c] Pr. Dr. M. Robert
Institut Universitaire de France (IUF)
F-75005, Paris, France

**Abstract:** Iron porphyrins are attractive catalysts for the electrochemical reduction of carbon dioxide ($CO_2$), owing to their high activity and selectivity, while being tunable through ligand functionalization. Iron tetraphenyl porphyrin (FeTPP) is the simplest of them and its catalytic behavior towards $CO_2$ has been studied for decades. Although kinetic information is available, spectroscopic signatures are lacking to describe intermediate species along the catalytic cycle. We have used *in situ* UV-Visible and X-ray absorption near edge spectroscopy (XANES) to monitor the local and electronic structure of FeTPP homogeneously disolved in dimethyl formamide (DMF) under reductive potentials. We identify the Fe(III) starting species, together with its one, two and three electron reduced counterparts under both argon and $CO_2$ atmospheres. Under argon, the second and third reductions lead to species with electronic density shared between the metal and the porphyrin backbone. In the presence of $CO_2$ and with a low amount of protons, the doubly and triply reduced species interact with $CO_2$ at the metallic site. In light of these results, we propose an electronic structure for a key intermediate along the catalytic cycle of the $CO_2$-to-CO reduction reaction.

## Introduction

The massive use of fossil fuels to supply the global energetic demand has increased the $CO_2$ atmospheric levels to alarming values, as recently presented by the Intergovernmental Panel on Climate Change (IPCC).[1] Research has shown that $CO_2$ can be electrochemically reduced into carbon building blocks such as carbon monoxide (CO), which is the first and most critical step in the $CO_2$ upcycling process. Because of the high chemical stability of $CO_2$,[2] the $CO_2$-to-CO conversion is energetically very costly, requiring the use of efficient catalysts to lower energetic barriers. Several molecular catalyst families based on earth-abundant transition metals have been proposed as efficient $CO_2$-to-CO reducing catalysts. They offer good catalytic activities, both in terms of efficiency and selectivity, and provide convenient platforms for molecular engineering.[3–5] Among them, iron porphyrins, such as iron tetraphenyl porphyrin (FeTPP, Figure 1A), have been reported as a class of selective, stable, and efficient catalysts for the reduction of $CO_2$ into CO, both in aprotic solvents and water.[6–12] Doris Lexa, together with Jean-Michel Savéant and their collaborators, pioneered the electrochemical study of iron porphyrins and their reduced counterparts as early as the 80's.[6,13,14] Using cyclic voltammetry (CV), they showed that, in dimethyl formamide (DMF) and under inert conditions, FeTPP undergoes three consecutive reduction processes (see figure 1B), which correspond to the reversible storage of three reducing equivalents. In the presence of $CO_2$, the third reduction process becomes irreversible and increases in intensity, which is due to the catalytic reduction of $CO_2$ into CO following equation 1:

$$CO_2 + 2e^- + 2H^+ \rightarrow CO + H_2O \quad (1)$$

Despite numerous investigations of the $CO_2$-to-CO reaction mechanism *via* kinetic analysis,[13–18] the exact nature and structure of the intermediate species involved still need to be deciphered. There is, however, no doubt that understanding the local and electronic structure of such intermediates is required to optimize their catalytic activity. In this regard, early work by Lexa and co-workers showed that the reactivity of the three-electron reduced species of iron porphyrins is centered on the metal rather than on the ligand.[19] These observations, associated with *in situ* UV-Vis, resonance Raman and EPR spectroelectrochemistry,[20–22] led to the conclusion that the three-electron reduced species should be considered as an Fe(0) complex. More recently, Römelt *et al.* proposed, on the basis of X-ray Absorption Near Edge Spectroscopy (XANES) performed on solid state samples and Density Functional Theory (DFT) calculations, that the second and third electrons injected in $[Fe^{III}TPP]^+$ are localized on the porphyrin ring rather than on the metal.[23] They therefore formulated the two- and three-electron reduced species as $[Fe^{II}TPP\bullet]^-$ and $[Fe^{II}TPP\bullet\bullet]^{2-}$.

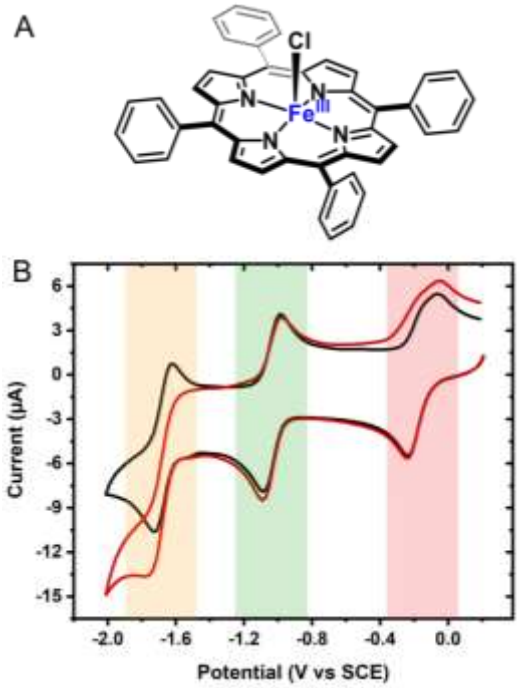


**Figure 1.** Structure (A) and cyclic voltamogram (B) of iron tetraphenyl porphyrin chloride [$Fe^{III}$TPP(Cl)] in DMF/$TBAPF_6$ (0.1 M) under Ar (black line) and $CO_2$ (red line). Colored areas indicate the first (red), second (green) and third (yellow) electron transfer processes. CVs were recorded in a conventional electrochemical cell at room temperature and a scan rate of $v$ = 100 mV $s^{-1}$.

As shown from this work and many others, XANES is an ideal tool to probe the local and electronic structure of transition metals.[24–27] It provides information on the oxidation state (through the main edge position) and on the geometry and spin state (through the shape and position of the pre-edge) of the element being probed. In combination with electrochemical techniques, it allows observing species that would otherwise be difficult to isolate. Such *in situ* measurements however require specific instrumentation to couple the two techniques. Up to now, spectroelectrochemical cells for X-ray spectroscopies were mostly developed for heterogeneous systems.[28–32] Unfortunately, *in situ/operando* analysis on immobilized materials lacks precision when it comes to identifying intermediates. Indeed, the high catalyst loading leads to a signal that can be dominated by inactive material rather than active one.[33] In addition, the electrochemical analysis of immobilized catalysts by cyclic voltammetry is challenging, with electron transfer processes being hidden by electrode effects. The stepwise generation of reduced intermediates on the way to catalytic potentials is therefore hampered, jeopardizing the identification of the catalytic species involved. On the contrary, the study of molecular catalysts in homogeneous conditions allows a better correlation with electrochemical measurements, thus providing more accurate information on the chemical state of the catalysts as a function of the electrode applied potential.

Herein, we present an *in situ* spectroelectrochemical study of the $CO_2$-reducing molecular electrocatalyst [$Fe^{III}$TPP(Cl)] in a DMF solution. We describe a custom-made vacuum compatible X-ray spectroelectrochemical flow cell for the *in situ* study of homogeneous systems in organic solvents and provide XANES and UV-Vis spectra relative to the four oxidation states involved in the redox process, both under argon and carbon dioxide atmospheres (as identified in Table 1).

**Table 1.** Identification of the species generated and studied in this study.

| $e^-$ transferred | Ar | $CO_2$ |
|---|---|---|
| 0 | **1** | **5** |
| 1 | **2a, 2b, 2c** | **6** |
| 2 | **3** | **7** |
| 3 | **4** | **8** |

## Results

### 1. A vacuum-compatible X-ray spectroelectrochemical flow cell for the study of homogeneous organic solutions.

A handful of cells have been reported for the study of electroactive species in solution with a thin-layer configuration,[34–37] with the possibility to flow the sample for some of them.[38–43] In order to study the FeTPP complex in DMF, we have developed a novel thin layer spectroelectrochemical flow cell suitable for X-ray spectroscopic experiments (see Figure 2 and Figures S1 and S2), inspired from the work of Jiang *et al.*[44] This cell allows performing *in situ* measurements in homogeneous conditions with organic solvents under primary vacuum.

Briefly, the cell consists of a main body made in polyether ether ketone (PEEK), a solvent-resistant polymer, to which two polytetrafluoroethylene (PTFE) tubes are connected as liquid inlet and outlet. The electrochemical chamber of the cell consists of a thin layer (200 µm) of liquid that can be circulated between a working (a 60 µm thick glassy carbon film) and a counter (platinum film) electrode. A reference electrode (silver pseudo-reference) is inserted from the side in the liquid path. The small cell volume ensures the total electrochemical conversion of the species of interest within a short time (< 5 min), preventing excessive X-ray dose and subsequent damage. It ensures a laminar flow of the circulating liquid, preventing the formation of bubbles and allowing a complete renewal of the sample.

To assess the behavior of the X-ray spectroelectrochemical cell, an initial study in the presence of iron chloride was carried out. Iron(III) chloride hexahydrate ($Fe^{III}Cl_3 \cdot 6H_2O$) and iron(II) chloride ($Fe^{II}Cl_2$) reference samples were considered due to previously reported XANES data in the solid state and aqueous solutions for these compounds.[41,45,46] Therefore, samples were prepared under anaerobic conditions in DMF and tetrabutylammonium hexafluorophosphate ($TBAPF_6$, 0.1 M) as supporting electrolyte.

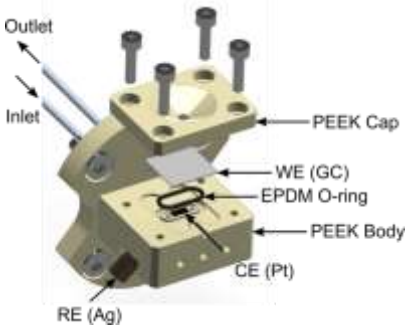


**Figure 2.** 3D scheme of the spectroelectrochemical cell. PEEK stands for "polyethylene ether ketone", WE for "working electrode", GC for "glassy carbon", EPDM for "ethylene propylene diene monomer", CE for "counter electrode" and RE for "reference electrode".

Fe K-edge XANES spectra were recorded *in situ* on both the $Fe^{III}$ and $Fe^{II}$ reference solutions. As shown in Figure 3, the spectrum of the $Fe^{III}$ sample (blue line) presents a low intensity white line (main edge peak top) as well as a pronounced pre-edge peak at 7114.6 eV (all pre-edge positions are measured at the peak top) and a main edge at 7122.3 eV (all main edge energies are measured at the half-edge jump, where the normalized intensity is equal to 0.5). The ferrous compound (Figure 3 – red line) presents a spectrum with a main edge that is shifted by 2 eV towards lower energies in comparison with the spectrum of the ferric compound (Figure 3 – blue line). Such a downshift in edge energy position is indicative of a reduction of the element probed. In addition, the intensity of the pre-edge peak clearly decreases and is also shifted towards lower energies to 7113.0 eV. The main edge energy shift, as well as the changes observed in the pre-edge intensities for the solutions of $Fe^{III}Cl_3$ and $Fe^{II}Cl_2$ are in agreement with previously reported data[46] and confirm an oxidation state difference of one unit between these two species. A cyclic voltammogram (CV) was performed in the spectroelectrochemical cell under Ar atmosphere (Figure 3, insert) on the $Fe^{III}Cl_3$ solution. The CV shows an anodic peak at -0.10 V and a cathodic peak at -0.22 V *vs.* $Ag/Ag^+$. When $Fe^{III}Cl_3$ is electrochemically reduced by applying a constant potential of –0.6 V *vs.* $Ag/Ag^+$ during approximately 15 minutes, the main edge energy of XANES spectrum shifts by 2 eV towards lower values (Figure 3 – dotted line). The spectrum obtained matches closely the one of the $Fe^{II}Cl_2$ reference sample. Linear combination fittings (LCF) were performed on the XANES spectrum of the final species, using the spectra of the $Fe^{III}Cl_3$ and $Fe^{II}Cl_2$ reference solutions, indicating a conversion of 96% from $Fe^{III}$ to $Fe^{II}$ (see Figure S3).

***2. In situ* XANES and UV-Vis spectroelectrochemistry of [$Fe^{III}$TPP(Cl)] and its reduced species under Ar atmosphere.**

The Fe K-edge XANES spectrum of an Ar saturated 2 mM solution of [$Fe^{III}$TPP(Cl)] (named **1**) in DMF/$TBAPF_6$ (0.1 M) was recorded and compared with the one of the solid sample (see Figure S4). The two spectra are very similar, indicating that, under these conditions, the chloride ligand remains bound to the metal center.

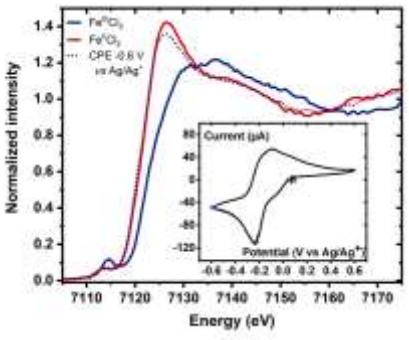


**Figure 3.** Fe K-edge XANES spectra recorded on 2 mM solution of $Fe^{III}Cl_3$ (blue line) and $Fe^{II}Cl_2$ (red line) in DMF/$TBAPF_6$ (0.1 M) under Ar atmosphere. The spectrum of the $Fe^{II}Cl_2$ species obtained after a 15 min constant potential electrolysis at -0.6 V *vs.* $Ag/Ag^+$ under the same conditions is also shown (dotted purple line). Insert: Cyclic voltammogram of the 2 mM solution of $Fe^{III}Cl_3 \cdot 6H_2O$ in DMF/$TBAPF_6$ (0.1 M) under Ar atmosphere recorded in the X-ray spectroelectrochemical cell ($v$ = 100 $mV.s^{-1}$, room temperature).

The cyclic voltammogram (CV) of the initial [$Fe^{III}$TPP(Cl)] complex recorded in the X-ray spectroelectrochemical cell (Figure 4A) in DMF/$TBAPF_6$ under Ar exhibits three well-defined reversible waves. They correspond to three consecutive one-electron reduction processes, ascribed to the $Fe^{III}/Fe^{II}$, $Fe^{II}/Fe^{I}$ and $Fe^{I}/Fe^{0}$ formal couples.[6,22] The initial UV-Vis spectrum of the [$Fe^{III}$TPP(Cl)] species presents a Soret band at $\lambda$ = 416 nm and Q-bands at $\lambda$ = 509 nm and 575 nm, which correspond to previously reported values in the same solvent.[22]

Controlled potential electrolysis (CPE) were performed at the potentials indicated by arrows in the CV shown on Figure 4A, *i.e.* -0.8 V, -1.6 V and -2.0 V *vs.* $Ag/Ag^+$, corresponding to the first, second and third electron reductions, respectively. Figure 4B shows the normalized Fe K-edge XANES spectra of the starting [$Fe^{III}$TPP(Cl)] species in DMF/$TBAPF_6$ 0.1 M and of the species obtained under various applied potentials. Measurements were performed when the electrolysis currents were stabilized (after *ca.* 2-5 min) and the possible occurrence of radiation-induced damages was carefully monitored.

The XANES spectra analysis of iron porphyrins may be divided into two different sections. First, a pre-edge region extending from 7111 to 7120 eV corresponds to transitions from the 1*s* to 3*d*/4*p* orbitals, while the main edge region from 7120 to 7140 eV corresponds to transitions from the 1*s* to the 4*p* orbitals.

*One electron reduction species.* The first reduction step was performed by applying a constant electrode potential of *ca*. -0.8 V *vs*. $Ag/Ag^+$. No energy shift was observed in the main edge of the Fe K-edge XANES spectrum upon reduction of [$Fe^{III}$TPP(Cl)] by one electron (named complex **2a**), as can be seen in Figure 4B. On the contrary, the UV-Vis spectroelectrochemical data recorded upon one electron reduction of [$Fe^{III}$TPP(Cl)] leads to a shift of the Soret band from $\lambda$ = 416 nm for the [$Fe^{III}$TPP(Cl)] complex to a sharp Soret band at $\lambda$ = 432 nm for the one electron reduced specie as well as to the evolution of the Q-band region into three peaks at $\lambda$ = 530, 565 and 603 nm respectively (see Figure 4C and Figure S5 for intermediate spectra).

As shown in the work of Wilson *et al*.,[47] $Fe^{II}$TPP can adopt three different spin states, namely, high spin (HS, S = 2), intermediate spin (IS, S = 1) and low spin (LS, S = 0). These three species exhibit very different main edge and pre-edge features in their Fe K-edge XANES spectra.

In order to confirm the nature of the species electrogenerated at -0.8 V *vs.* $Ag/Ag^+$, we synthesized the [$Fe^{II}$TPP] species by chemical reduction of [$Fe^{III}$TPP(Cl)], as previously described, generating **2b**.[23,48] When compared with the spectrum of the initial [$Fe^{III}$TPP(Cl)] complex, the main edge position of the chemically reduced solid sample (see Figure S6) shows a 2 eV shift towards lower energies (from 7123.0 to 7121.0 eV). It also presents a high intensity shoulder at around 7118.0 eV, which corresponds to a low-lying 1s to $4p_z$ transition, as previously suggested by Römelt and co-workers.[23] These features indicate that **2b** in the solid state is in a four-coordinated, square planar environment with an intermediate spin (S = 1), as previously discussed.[23,47] The spectrum of this chemically reduced species is very different from that of complex **2a**, indicating that the two species have different spin states arising from the presence of DMF solvent molecule(s) in the coordination sphere of the complex generated in homogeneous conditions. Indeed, the loss of the feature at around 7118.0 eV in the electrogenerated species shows that the

$4p_z$ orbital is shifted towards higher energies due to axial coordination of DMF. To confirm this interpretation, we dissolved the chemically reduced [$Fe^{II}$TPP] solid sample in DMF under anaerobic conditions (named complex **2c**) and got a new spectrum that closely matches the one of the electrochemically reduced species (**2a**). These results illustrate that DMF plays a critical role in the electronic structure of the [$Fe^{III}$TPP(Cl)] species. Consistent with previously reported data,[47] **2a** and **2c** are in a low-spin (S = 0) configuration, while **2b** is in an intermediate spin (S = 1) configuration. Such change in spin configuration explains the similarity between the XANES spectra of [$Fe^{III}$TPP(Cl)] and **2b** (generated electrochemically *in situ*), the edge shift towards lower energies expected from the reduction of Fe(III) to Fe(II) being compensated by an upshift due to the spin change.

*Two and three electrons reduced species*. The second reduction step was performed by applying constant electrode potential of *ca*. -1.6 V *vs.* $Ag/Ag^+$ to obtain the [$Fe^{III}$TPP(Cl)] + $2e^-$ species (named **3**). As observed in Figure 4B, the main edge energy is slightly shifted to lower values (0.7 eV) when compared to the initial sample, while the pre-edge feature increases in intensity. In addition, a low intensity shoulder appears at *ca*. 7118.0 eV. The presence of this feature, arising from a 1*s* to $4p_z$ transition (similar to the one found in the intermediate spin [$Fe^{II}$TPP] species), points towards a square planar environment around the Fe center. The UV-Vis spectroelectrochemical data recorded upon reduction of [$Fe^{II}$TPP(Cl)] by a second electron leads to a decrease in intensity and splitting of the Soret band, with two peaks at $\lambda$ = 392 nm and $\lambda$ = 425 nm (see Figure 4C and S5 for intermediate spectra). The Q-bands of **3** present three bands located at $\lambda$ = 510 nm, 575 nm and 608 nm, respectively. These results are in line with previously reported data on complex **3**.[21]

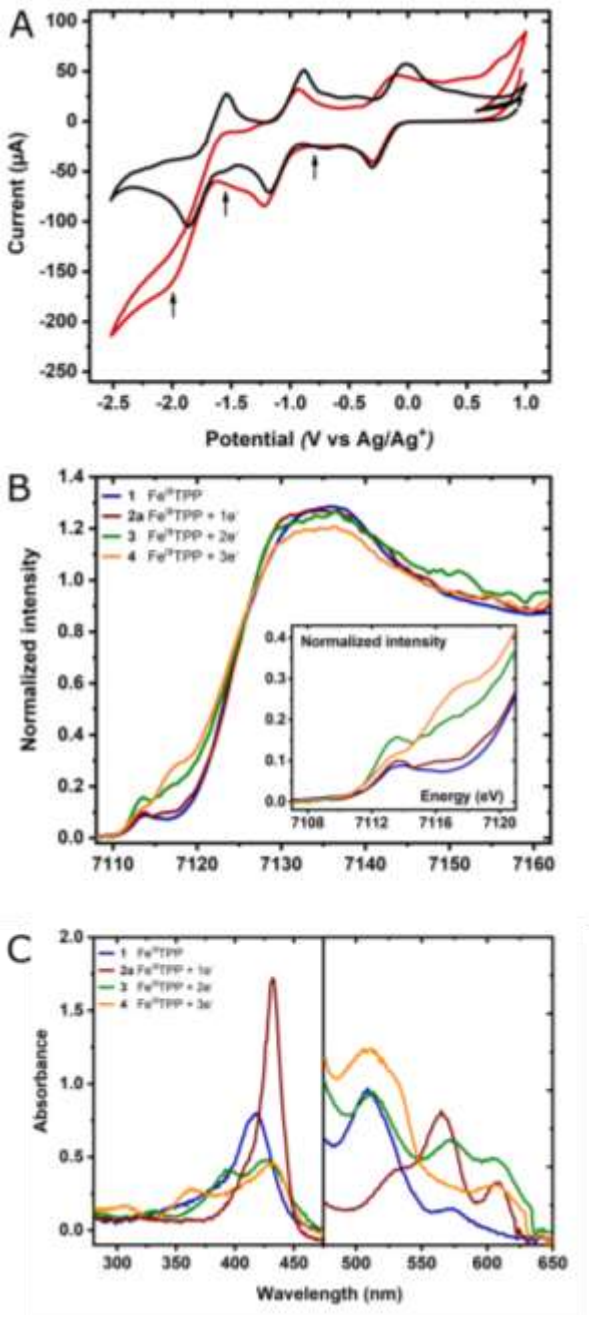


**Figure 4. A.** Cyclic voltammogram of a 2 mM solution of [$Fe^{III}$TPP(Cl)] in DMF/$TBAPF_6$ (0.1 M) under Ar recorded in the X-ray spectroelectrochemical cell at $v$ = 100 $mV.s^{-1}$ (room temperature). Reduction potentials applied during spectroelectrochemical measurements are indicated by black arrows. **B.** Fe K-edge XANES spectra recorded on [$Fe^{III}$TPP(Cl)] solution, under the conditions described above (blue) and while applying a constant potential of E = -0.8 V (red), -1.6 V (green) and -2.0 V *vs.* $Ag/Ag^+$ (orange). **C.** UV-Vis spectra (Soret Bands, left, Q-bands, right) for a solution of [$Fe^{III}$TPP(Cl)] in DMF/$TBAPF_6$ (0.1 M) under Ar (blue) and electrochemically reduced at E = -0.8 V (red), -1.6 V (green) and -2.0 V (orange) *vs.* $Ag/Ag^+$ respectively.

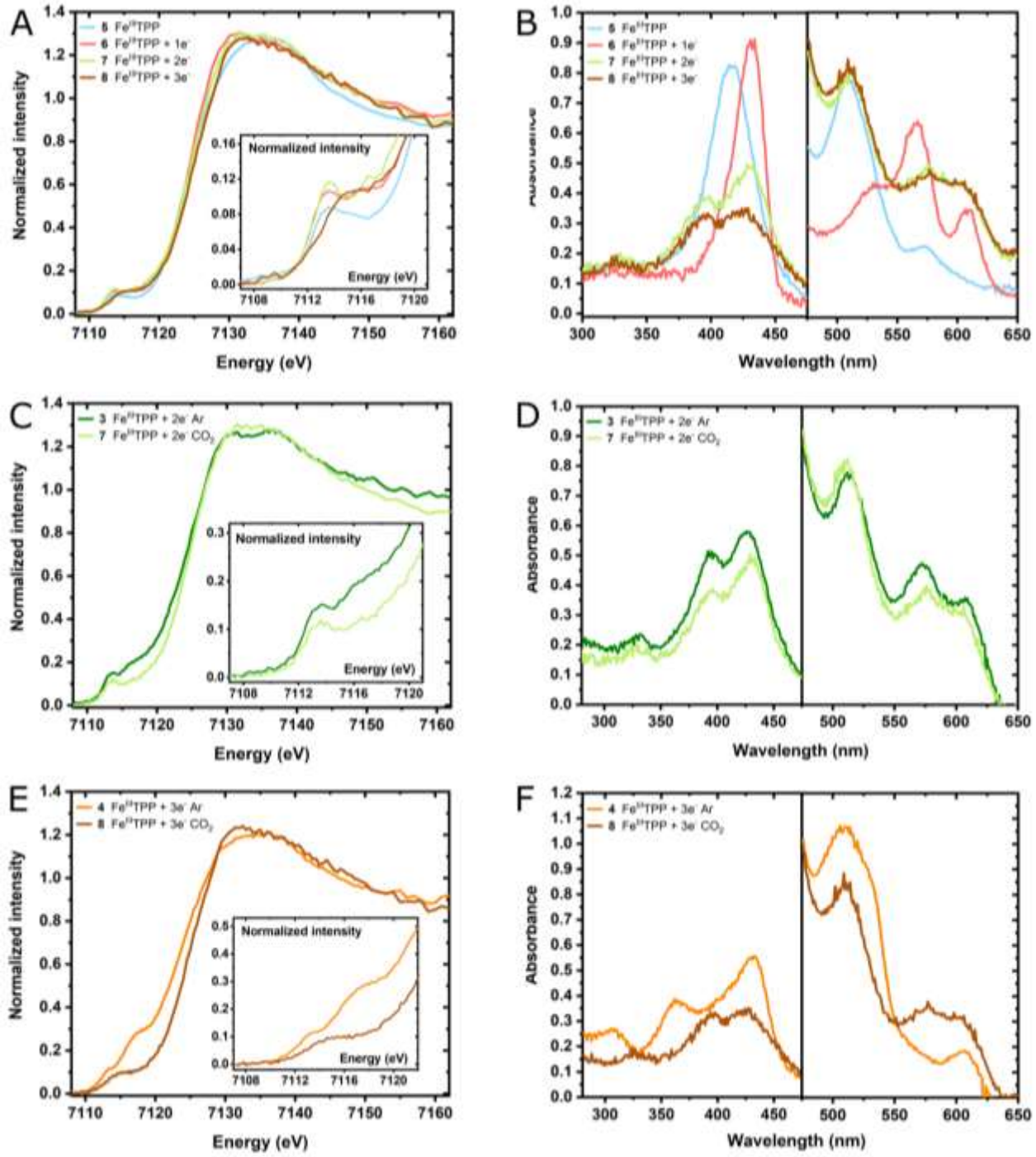


**Figure 5. A.** Fe K-edge XANES spectra recorded on a 2 mM solution of [Fe$^{III}$TPP(Cl)] in DMF/TBAPF$_6$ (0.1 M) under $CO_2$ (light blue) and while applying a constant electrode potential of E = -0.8 V (magenta), -1.6 V (light green) and -2.0 V (brown) *vs.* Ag/Ag$^+$ respectively. **B.** UV-Vis spectra (Soret Bands on the left, Q-bands on the right) of [Fe$^{III}$TPP(Cl)] in DMF/ TBAPF$_6$ (0.1 M) under $CO_2$ (light blue) and while applying a constant electrode potential of E = -0.8 V (magenta), -1.6 V (light green) and -2.0 V (brown) *vs.* Ag/Ag$^+$. **C**. Comparison of the Fe K-edge XANES and **D.** UV-Visible spectra recorded after controlled potential electrolysis at -1.6 V *vs.* Ag/Ag$^+$ under Ar (green) and $CO_2$ (light green), respectively. **E**. Comparison of the Fe K-edge XANES and **F.** UV-Visible spectra recorded upon applying a constant electrode potential of E = -2.0 V *vs.* Ag/Ag$^+$ under Ar (orange) and $CO_2$ (brown).

Finally, a third reduction step is carried out by applying a constant electrode potential of *ca.* -2.0 V *vs.* Ag/Ag$^+$ (formation of the species named **4**). The spectrum (see Figure 4B) shows a shift of the main edge position of *ca*. 0.3 eV towards lower values when compared with the 2e$^-$ reduced species, indicating further reduction of the system. The pre-edge feature at 7113.6 eV decreases in intensity with respect to **3**, while the shoulder at *ca.* 7118.0 eV grows significantly. This increased intensity indicates a higher contribution of 4$p_z$ character in the final molecular orbitals of the 1$s$ $\rightarrow$ 4$p_z$ transition. The UV-Vis spectroelectrochemical data recorded on complex **4** leads to slight shifts of the Soret bands to $\lambda$ = 362 nm and 433 nm (see Figure 4C and Figure S5 for intermediate spectra). More important modifications are observed in the Q-band region, with the presence of a broad band

at $\lambda$ = 514 nm. These values are in line with those previously reported for **4** in DMF.[21,22]

### 3. *In situ / operando* XANES and UV-Vis spectroelectrochemistry of [Fe$^{III}$TPP(Cl)] and its reduced species under $CO_2$ atmosphere.

*One electron reduced species.* Figure 4A shows the comparison between the CVs obtained for the initial [Fe$^{III}$TPP(Cl)] complex in DMF/TBAPF$_6$ (0.1 M) under Ar (black line) and $CO_2$ (red line) atmospheres. Under $CO_2$, the third reduction wave presents a current increase and a loss of reversibility as compared to the one in Ar atmosphere, indicating a catalytic process. Although a proton source is usually required to catalyze the $CO_2$RR such as protons from residual water, $CO_2$ itself can play the role of a Lewis acid and lead to catalysis.[9,15]

Figure 5A shows the normalized Fe K-edge XANES spectra recorded *in situ* on [Fe$^{III}$TPP(Cl)] and its reduced species under $CO_2$ atmosphere, while Figure 5B shows the corresponding UV-Vis spectra (see Figure S7 for intermediate spectra). A comparison of the XANES spectrum of the initial [Fe$^{III}$TPP(Cl)] complex and its one electron reduced species under $CO_2$ atmosphere (**5** and **6** respectively) with the ones obtained in the presence of Ar (see Figures S8-9) shows that they are identical, indicating that there are no interactions between $CO_2$ and the Fe metal center at these oxidation states. This is confirmed by the UV-Visible spectra of [Fe$^{III}$TPP(Cl)] and its one-electron reduced species, which are comparable to their counterparts in Ar.

*Two and three electrons reduced species.* Further reduction of **6** with a second electron under $CO_2$ atmosphere (complex **7**) yields a XANES spectrum that is almost identical to the one of **6**. It presents, however, clear differences with the one of **3**, obtained under Ar, as can be seen in Figure 5C. The shoulder around 7118.0 eV is absent in the spectrum recorded under $CO_2$, which indicates that the square planar geometry observed under Ar has changed, hence pointing towards an interaction between $CO_2$ and the Fe center. It is worth mentioning that an interaction between $CO_2$ and an Fe(I) porphyrin was recently reported,[49] although in a different solvent (acetonitrile). The UV-Vis spectra of complex **7** presents a similar Soret band splitting as the one observed under Ar, with peaks at $\lambda$ = 392 nm and 425 nm. Q-bands were also located at the same position than those obtained under Ar, *i.e.* at $\lambda$ = 510 nm, 575 nm, 608 nm, 667 nm and 712 nm.

A XANES spectrum was recorded after the catalytic wave, at -2.0 V *vs.* Ag/Ag$^+$, where [Fe$^{III}$TPP(Cl)] is reduced with three electrons to yield complex **8**. Significant changes are observed in the pre-edge region when compared with the two electrons reduced species **7** (Figure 5A), but also with the three-electron reduced species under Ar, **4** (Figure 5E). The pre-edge region of the XANES spectrum is clearly different, not only with the disappearance of the shoulder at 7118.0 eV, but also with a shift of the pre-edge peak from 7113.6 eV eV (under Ar) to 7115.0 eV (under $CO_2$). It indicates an important structural modification around the metal center at this potential, pointing towards the coordination of $CO_2$ to the iron center. Moreover, the main edge position shifts to higher energies by *ca.* 0.7 eV when compared with the two-electron-reduced species in $CO_2$. This shift is even more pronounced when the spectra of the three-electron reduced species obtained under Ar (7122.0 eV) and $CO_2$ (7123.7 eV) are compared, with a shift to higher energies of 1.7 eV for the species obtained in $CO_2$. These data further support a coordination of $CO_2$ to the Fe center, which donates part of its electronic density to the incoming coordinating molecule and therefore appears as being less electron rich. The UV-Vis spectra of the species obtained after reduction of [Fe$^{III}$TPP(Cl)] with three electrons looks almost identical to the one obtained for the two-electron reduced species. The spectrum is, however, significantly different from its counterpart observed under Ar atmosphere (see Figure 5F).

## Discussion

The pre-edge and main edge positions of the XANES data as well as the peak positions of the UV-Visible Soret and Q-bands regions of compounds **1-8** are summarized in Table 2.

**Table 2.** XANES pre-edge and main edge energy positions (in eV) and UV-Visible peak positions (in nm) for compounds **1-8** .

| e$^-$ transferred | Complex | Pre-edge* | Main edge‡ | Soret band(s) | Q-band(s) |
|---|---|---|---|---|---|
| **Ar** saturated solution | | | | | |
| 0 | **1** | 7113.9 | 7123.0 | 416 | 509, 575 |
| 1 | **2a** | 7113.6 | 7123.0 | 432 | 530, 565, 603 |
| 2 | **3** | 7113.5, 7118 | 7122.3 | 392, 425 | 510, 575, 608 |
| 3 | **4** | 7113.6, 7118 | 7122.0 | 362, 433 | 514, 607 |
| **$CO_2$** saturated solution | | | | | |
| 0 | **5** | 7113.9 | 7123.0 | 417 | 508, 575 |
| 1 | **6** | 7113.6 | 7123.0 | 430 | 535, 567, 609 |
| 2 | **7** | 7113.5 | 7123.0 | 392, 425 | 510, 575, 608 |
| 3 | **8** | 7115.0 | 7123.7 | 395, 424 | 510, 575, 608 |

* The pre-edge peak positions are measured at the peak maximum.

‡ The main edge positions are measured at the half-edge jump (normalized intensity = 0.5).

*Electronic structure under Ar.* The XANES data collected on the two and three electrons reduced species of [$Fe^{III}$TPP(Cl)] under Ar show slight shifts of the main edge energy towards lower values, as more electrons are injected in the complex. These shifts are notably small (-0.7 and -0.3 eV) and cannot be assigned to full oxidation state changes, suggesting a partial localization of the electrons both on the metal and on the porphyrin ligand. As previously mentioned, the pre-edge feature observed at 7118.0 eV can be attributed to a $1s \rightarrow 4p_z$ transition. This peak appears in the [$Fe^{II}$TPP] complex in the solid state, which does not have apical ligands and adopts a square planar geometry, leading to an intermediate spin configuration. When dissolved in solution, one or two DMF molecule(s) coordinate the metal, and the feature at 7118.0 eV disappears due to a square (bi)pyramidal structure. When the complex is reduced with a second electron, the shoulder at 7118.0 eV appears with a low intensity, which can be explained by a repulsion of the DMF molecule(s) by the charge (-1) appearing on the Fe porphyrin. Further reduction by a third electron and increase of the charge (-2) lead to the removal of the DMF apical ligands, thus generating a square planar geometry similar to what that observed for the $Fe^{II}$ complex in the solid state, as attested by the presence of the $1s \rightarrow 4p_z$ transition.
Taken together, this *in situ* dataset indicates that the one-electron reduced species of [$Fe^{III}$TPP(Cl)] in DMF is a low spin Fe(II) complex, while the two and three electrons reduced species have an electronic structure where the additional electrons are shared between the metal and the porphyrin.

*Electronic structure under $CO_2$.* Under $CO_2$ atmosphere, significant differences are observed in the XANES spectra with respect to the Ar atmosphere conditions. The two-electron reduced species (complex **7**) presents a XANES spectrum that is different from the one in Ar, with a pre-edge region that misses the shoulder at 7118.0 eV, indicating a deviation from the square planar geometry and thus suggesting an interaction with $CO_2$. The UV-Vis spectrum obtained under these conditions is, however, almost identical to the one obtained under Ar. This difference may be explained by the lower sensitivity of UV-Vis to valence-level electronic changes. It also suggests that the interaction between **7** and $CO_2$ is very loose and that no bond is formed with the metallic center.
When reduced with a third electron, more prominent differences can be observed, both by XANES and UV-Visible spectroscopy, when compared to the Ar atmosphere conditions (complexes **8** *vs.* **4,** Figure 5E-F). The pre-edge region of the XANES spectrum is clearly different, not only with the disappearance of the shoulder at 7118.0 eV, but also with a shift of the pre-edge peak from 7113.6 eV (under Ar) to 7115.0 eV (under $CO_2$). Moreover, the main edge position lies 1.7 eV higher than under Ar. The UV-Visible data show clear differences with the one obtained under Ar, but looks actually very similar to those obtained with **3** and **7**, the doubly reduced species observed under Ar or $CO_2$, respectively. Therefore, both the XANES and UV-Visible data for complex **8** show differences with respect to those obtained under Ar (complex **4**), indicating that $CO_2$ is bound to the iron center. The disappearance of the peak at 7118.0 eV in the pre-edge region of the XANES spectrum supports a deviation from the square-planar geometry, consistent with a square pyramidal geometry with $CO_2$ bound to Fe center and sitting on top of the porphyrin plane. The UV-Visible spectrum of **8** is very similar to that **3**, which is only reduced with two electrons (*vs.* three electrons for **8**). This suggest an electronic structure for **8** where part of the electronic density is delocalized between the metalloporphyrin system and the $CO_2$ substrate.

*$CO_2$ reduction mechanism.* The cyclic voltammetry experiments shown in Figure 4A indicate that $CO_2$ reduction catalysis occurs at the third reduction wave (*ca.* -1.8 V *vs.* $Ag/Ag^+$), thanks to the presence of a residual source of protons (and/or with a second $CO_2$ molecule acting as a Lewis acid to help C-O bond breaking). In such low proton availability conditions, the rate determining step of the $CO_2$ reduction reaction is the cleavage of the OC-O bond (see figure 6).[18] In other words, the species expected to be observed under these catalytic conditions is the one accumulating before the rate-limiting step, *i.e.* the triply reduced FeTPP species with $CO_2$ bound to the metal. The comparison of the *in situ* XANES and UV-Visible data collected under Ar or $CO_2$ atmospheres provide direct evidence for the coordination of $CO_2$ to the Fe in the triply reduced form of [$Fe^{III}$TPP(Cl)]. These results are consistent with the $CO_2$-to-CO mechanism considered so far (see Scheme S1) and unambiguously demonstrate that, despite an electronic density partly localized on the porphyrin ligand, the reactivity of the triply reduced iron porphyrin towards $CO_2$ indeed occurs at the metallic center. It implies that the localization of the electronic density is partly shifted from the metalloporphyrin organic backbone to the metal center upon substrate coordination. This behavior may explain the ability of iron porphyrins to store electrons without reacting, until a substrate molecule is activated.

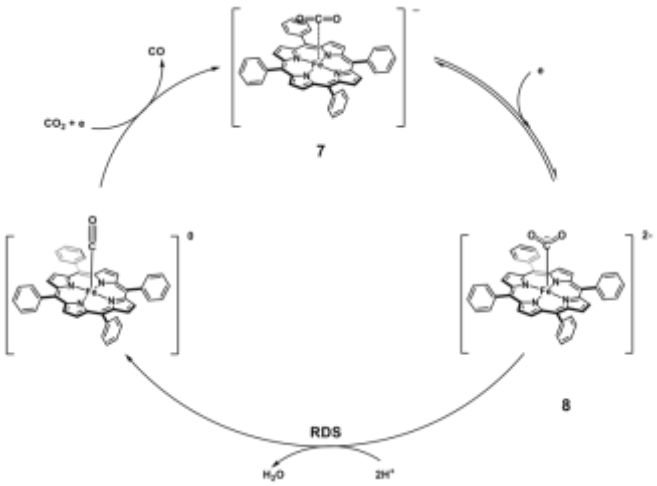


**Figure 6.** Simplified catalytic cycle for the electrochemical reduction of $CO_2$ into CO by FeTPP in DMF with the identification of species 7 and 8.

## Conclusion

Using a custom made *in situ* X-ray spectroelectrochemical cell, we collected the XANES spectra of the [$Fe^{III}$TPP(Cl)] complex in a DMF homogeneous solution, together with its one, two and three electrons reduced species. These data were collected both under Ar and $CO_2$ atmospheres and correlated with the corresponding UV-Vis spectroelectrochemical data. We showed that, when dissolved in DMF, the one electron reduced species is an Fe(II) complex with a low spin electronic configuration, due to the coordination of DMF to the central Fe ion. The two and three electrons reduced species generated under Ar are proposed to have electronic structures where the electron density is shared between the metal and the porphyrin ring. Under $CO_2$ atmosphere,

the XAS and UV-Vis spectra collected *in situ* show new features, which indicate that (i) $CO_2$ is loosely bound to the two electrons reduced species and (ii) $CO_2$ is coordinated to the iron center in the triply reduced iron porphyrin species, which is the active form of the catalyst. This result is consistent with a rate-limiting step of the reaction corresponding to the cleavage of the OC-O bond and indicate that reactivity towards $CO_2$ occurs on the metallic center rather on the ligand. Overall, these findings provide a better understanding of the electrocatalytic mechanism for $CO_2$ reduction with molecular catalysts.

## Acknowledgements

We are indebted to the Michem Labex and Synchrotron SOLEIL for a PhD grant to D. M. The peer-review committees of Synchrotron SOLEIL are greatly acknowledged for beamtime allocation. MR is thankful to the Institut Universitaire de France (IUF) for partial financial support. O. R-W acknowledges financial support from the *Investissement l'Avenir* through the *MOPGA* call Nº ANR-18-MPGA-0012.

**Keywords:** $CO_2$ reduction • Spectroelectrochemistry • X-Ray absorption spectroscopy • porphyrins • electronic structure

## References

(1) Masson-Delmotte, V., Zhai, P.; Pirani, A.; Connors, S.L.; Péan, C.; Berger, S.; Caud, N.; Chen, Y.; Goldfarb, L.; Gomis, M.I.; Huang, M.; Leitzell, K.; Lonnoy, E.; Matthews, J.B.R.; Maycock, T.K.; Waterfield, T.; Yelekçi, O.; Yu, R and Zhou, B (eds.) IPCC, **2021**: Summary for policymakers. In: Climate Change 2021: The physical science basis. Contribution of working group I to the sixth assessment report of the Intergovernmental panel on Climate Change. Cambridge University Press. In Press.
(2) Lamy, E.; Nadjo, L.; Savéant, J.-M. *J. Electroanal. Chem. Interf. Electrochem.* **1977**, *78* (2), 403–407.
(3) Collin, J. P.; Sauvage, J.-P. *Coord. Chem. Rev.* **1989**, *93* (2), 245–268.
(4) Kinzel, N. W.; Werlé, C.; Leitner, W. T. *Angew. Chem. Int. Ed.* **2021**, *60* (21), 11628–11686.
(5) Boutin, E.; Merakeb, L.; Ma, B.; Boudy, B.; Wang, M.; Bonin, J.; Anxolabéhère-Mallart, E.; Robert, M. *Chem. Soc. Rev.* **2020**, *49* (16), 5772–5809.
(6) Hammouche, M.; Lexa, D.; Savéant, J-M.; Momenteau, M. *J. Electroanal. Chem. Interf. Electrochem.* **1988**. 249, 347-351.
(7) Costentin, C.; Drouet, S.; Robert, M.; Savéant, J.-M. *Science* **2012**, *338* (6103), 90–94.
(8) Gotico, P.; Roupnel, L.; Guillot, R.; Sircoglou, M.; Leibl, W.; Halime, Z.; Aukauloo, A. *Angew. Chem. Int. Ed.* **2020**, *59* (50), 22451–22455.
(9) Costentin, C.; Robert, M.; Savéant, J.-M.; Tatin, A. *Proc Natl Acad Sci USA.* **2015**, *112* (22), 6882–6886.
(10) Azcarate, I.; Costentin, C.; Robert, M.; Savéant, J.-M. *J. Am. Chem. Soc.* **2016**, *138* (51), 16639–16644.
(11) Gotico, P.; Boitrel, B.; Guillot, R.; Sircoglou, M.; Quaranta, A.; Halime, Z.; Leibl, W.; Aukauloo, *Angew. Chem. Int. Ed.* **2019**, *58* (14), 4504–4509.
(12) Khadhraoui, A.; Gotico, P.; Boitrel, B.; Leibl, W.; Halime, Z.; Aukauloo, A. *Chem. Comm.* **2018**, *54* (82), 11630–11633.
(13) Hammouche, M.; Lexa, D.; Momenteau, M.; Savéant, J.-M. *J. Am. Chem. Soc.* **1991**, *113* (22), 8455–8466.
(14) Bhugun, I.; Lexa, D.; Savéant, J.-M. *J. Am. Chem. Soc.* **1994**, *116* (11), 5015–5016.
(15) Bhugun, I.; Lexa, D.; Savéant, J.-M. *J. Am. Chem. Soc.* **1996**, *118* (7), 1769–1776.
(16) Costentin, C.; Passard, G.; Robert, M.; Savéant, J.-M. *J. Am. Chem. Soc.* **2014**, *136* (33), 11821–11829.
(17) Bhugun, I.; Lexa, D.; Savéant, J.-M. *J. Phys. Chem.* **1996**, *100* (51), 19981–19985.
(18) Costentin, C.; Drouet, S.; Passard, G.; Robert, M.; Savéant, J.-M. *J. Am. Chem. Soc.* **2013**, *135* (24), 9023–9031.
(19) Lexa, D.; Savéant, J-M.; Li Wang, D. *Organometallics*. **1986**. 5, 7, 1428-1434.
(20) Gueutin, C.; Lexa, D. *Electroanalysis* **1996**, *8* (11), 1029–1033.
(21) Anxolabéhère, E.; Chottard, G.; Lexa, D. *New. J. Chem*. **1994**. 18, 889-899.
(22) Lexa, D.; Momenteau, M.; Mispelter, J. *Biochim. Biophys. Acta.* **1974**, *338* (1), 151–163.
(23) Römelt, C.; Song, J.; Tarrago, M.; Rees, J. A.; van Gastel, M.; Weyhermüller, T.; DeBeer, S.; Bill, E.; Neese, F.; Ye, S. *Inorg. Chem.* **2017**, *56* (8), 4745–4750.
(24) Kowalska, J.; DeBeer, S. *Biochim. Biophys. Acta.* **2015**, *1853* (6), 1406–1415.
(25) Lassalle-Kaiser, B.; Gul, S.; Kern, J.; Yachandra, V.; Yano, *J. Electron. Spectrosc. Relat. Phenom*. **2017**. 221, 18-27.
(26) Yano, J.; Yachandra, V. K. *Photosynth Res.* **2009**, *102* (2–3), 241–254.
(27) Timoshenko, J.; Roldan Cuenya, B. *Chem. Rev.* **2021**, *121* (2), 882–961.
(28)Xuan, G.; Jang, S; Kwang, G.; Sunghyun K. *Bull. Korean. Chem. Soc.* **2005**, *26* (4), 671–674.
(29) Nakanishi, K.; Kato, D.; Arai, H.; Tanida, H.; Mori, T.; Orikasa, Y.; Uchimoto, Y.; Ohta, T.; Ogumi, Z. *Rev. Sci. Instrum.* **2014**, *85* (8), 084103.
(30) León, L.; Mozo, J. D. *Trends Analyt Chem.* **2018**, *102*, 147–169.
(31) Weng, Z.; Wu, Y.; Wang, M.; Jiang, J.; Yang, K.; Huo, S.; Wang, X.-F.; Ma, Q.; Brudvig, G. W.; Batista, V. S.; Liang, Y.; Feng, Z.; Wang, H. *Nat. Comm.* **2018**, *9* (1), 1–9.
(32) Lassalle-Kaiser, B.; Zitolo, A.; Fonda, E.; Robert, M.; Anxolabéhère-Mallart, E. *ACS Energy Lett.* **2017**, *2* (11), 2545–2551. 9.
(33) King, H. J.; Fournier, M.; Bonke, S. A.; Seeman, E.; Chatti, M.; Jumabekov, A. N.; Johannessen, B.; Kappen, P.; Simonov, A. N.; Hocking, R. K. *J. Phys. Chem. C* **2019**, *123* (47), 28533–28549.
(34) Dewald, H. D.; Watkins, J. W.; Elder, R. C.; Heineman, W. R. *Anal. Chem.* **1986**, *58* (14), 2968–2975.
(35) Charnock, J. M.; Collison, D.; Garner, C. D.; McInnes, E. J. L.; Mosselmans, J. F. W.; Wilson, C. R. *J. Phys. IV.* **1997**, *7* (C2), C2-658.
(36) Ascone, I.; Cognigni, A.; Giorgetti, M.; Berrettoni, M.; Zamponi, S.; Marassi, R. *J. Synchrotron Rad*. **1999**. 6, 384-386.
(37) Anxolabéhère-Mallart, E.; Glaser, T.; Frank, P.; Aliverti, A.; Zanetti, G.; Hedman, B.; Hodgson, K. O.; Solomon, E. I. *J. Am. Chem. Soc.* **2001**, *123* (23), 5444–5452.
(38) Nappini, S.; D'Amario, L.; Favaro, M.; Dal Zilio, S.; Salvador, F.; Betz-Güttner, E.; Fondacaro,, A.; Píš, I.; Romanzin, L.; Gambitta, A.; Bondino, F.; Lazzarino, M.; Magnano, E. *Rev. Sci. Inst*. **2020**. 92, 015115.
(39) Ambrosi, A.; Sheng Shi, R. R.; D. Webster, R. *J. Mat. Chem. A.* **2020**. 8, 21902-21929.
(40) Achilli, E.; Minguzzi, A.; Visibile, A.; Locatelli, C.; Vertova, A.; Naldoni, A.; Rondinini, S.; Auricchio, F.; Marconi, S.; Fracchia, M.; Ghigna, P. *J Synchrotron Rad.* **2016**, *23* (2), 622–628.
(41) Cheaib, K.; Maurice, B.; Mateo, T.; Halime, Z.; Lassalle-Kaiser, B. *J Synchrotron Rad.* **2019**, *26* (6), 1980–1985.
(42) Tesch, M. F.; Bonke, S. A.; Golnak, R.; Xiao, J.; Simonov, A. N.; Schlögl, R. *Electrochem Sci Adv*. **2021**, e2100141.
(43) Nagasaka, M.; Yuzawa, H.; Horigome, T.; Kosugi, N. *Rev. Sci. Inst*. **2014**. 85, 104105.
(44) Jiang, P.; Chen, J.-L.; Borondics, F.; Glans, P.-A.; West, M. W.; Chang, C.-L.; Salmeron, M.; Guo, J. *Electrochem Comm.* **2010**, *12* (6), 820–822.
(45) Westre, T. E.; Kennepohl, P.; DeWitt, J. G.; Hedman, B.; Hodgson, K. O.; Solomon, E. I. *J. Am. Chem. Soc*. **1997**, 119, 27, 6297-6314.
(46) Apted, M. J.; Waychunas, G. A.; Brown, G. E. *Geochim Cosmochim Acta.* **1985**, *49* (10), 2081–2089.
(47) Wilson, S. A.; Green, E.; Mathews, I. I.; Benfatto, M.; Hodgson, K. O.; Hedman, B.; Sarangi, R. *Proc Natl Acad Sci U S A.* **2013**, *110* (41), 16333–16338.
(48) Mashiko, T.; Reed, C. A.; Haller, K. J.; Scheidt, W. R. *Inorg. Chem.* **1984**, *23* (20), 3192–3196.
(49) Masaoka, S.; Kosugi, K.; Kondo, M. *Angew Chem Int Ed.* **2021**. 60,40, 22070-22074.